Identification and validation of autophaggen-based nomograms to predict the prognostic value of patients with cervical cancer

Jinqun Jiang[1],HongYan Xu[2] PingShen Zhao[1] Hai Lu[3]

[1]Department of Clinical Laboratory, Yuebei People's Hospital, Shaoguan, Guangdong Province 512026 P.R. China;[2]Department of gynaecology, Yuebei People's Hospital, Shaoguan, Guangdong Province 512026 P.R. China;[3] Department of Breast diease, Guangdong Provincial Hospital of Chinese Medicine, Guangzhou University of Chinese Medicine, Guangzhou,Guangdong Province 510282 P.R. China.

Corresponding author:

Hai Lu MD

Department of Breast Disease, Guangdong Provincial Hospital of Chinese Medicine, Guangzhou University of Chinese Medicine, No. 55, West Ring Road, Guangdong Province 510282 P.R. China;

Mobile: +86 13415659780

Email: luhai@gzucm.edu.cn

ABSTRACT

Cervical cancer is a common malignancy in women and has a poor prognosis.More and more studies have shown that autophagy disorder is closely related to the occurrence of tumors. However, the prognostic role of autophagy gene in cervical cancer is still unclear. In this study, we constructed the risk signatures of autophagy related genes to predict the prognosis of cervical cancer. The expression profiles and clinical information of autophagy gene sets were downloaded from the TCGA and GES52903 queues as training sets and validation sets. The cervical normal tissue expression profile data from UCSC XENA website is GTEx data as a supplement to TCGA normal cervical tissue. Univariate COX regression analysis of 17 different autophagy genes with the Consensus approach tumor samples from the TCGA is divided into six subtypes, and the clinical traits in the six subtypes have different distribution, with further then absolute shrinkage and selection operator (LASSO) and multiariable COX regression method finally got seven autophagy genetic risk model is constructed, in the training set, the survival rate of high risk group is lower than the low risk group ($p < 0.0001$), the validation set,The AUC area of the receiver operating characteristic (ROC) curve, the training set is 0.894, and the verification set is 0.736. We find that the high and low risk score is closely related to the TMN stage (All P is less than 0.05).The nomogram shows that the risk score combined with other indicators such as age, G,T,M, and N better predicts 1-year, 2-year, 3-year survival, and the DCA curve shows that the risk model combined with other indicators produces better clinical efficacy.Then immune cells in 28 in the enrichment score, there were statistically significant differences, high and low risk most GSEA enrichment analysis, the main enrichment in G2 / M checkpoint high-risk score, Genes defining epithelial and mesenchymal transition, raised in response to the low oxygen levels (hypoxia) gene, gene is important to the mitotic spindle assembly, these are closely related with the occurrence of tumor . In conclusion, our constructed autophagy risk signature may be a prognostic tool for cervical

 doi:10.20944/preprints202008.0476.v1

cancer.

Keywords: cervical cancer, Autophagy, Predict, Prognostic, value

INTRODUCTION

Cervical cancer is the most common malignancy of the female reproductive tract, diagnosed in more than millions of women each year and causing 300,000 deaths worldwide[1]. Among women, it ranks fourth in mortality and morbidity[2]. Because the early symptoms of cervical cancer are not obvious, late lymph node metastasis is easy to occur, so the prognosis is poor. Currently the main treatment is surgery or chemical radiation[3].Therefore, revealing the molecular mechanism of cervical cancer can provide a new target for its diagnosis and improve the prognosis of patients.

Autophagy is a process of self-phagocytosis. It forms autophagosomes with lysosomes by wrapping its cytoplasmic proteins or organelles to clear its wrapped contents and achieve self-renewal[4], Autophagy is also one of the most important cytoplasmic recycling mechanisms[5]. Autophagy is closely related to the occurrence of cancer, Cancer cells rely on systemic autophagy in their cytoplasm and in the host to sustain growth[6], Autophagy provides the necessary nutrients and raw materials for the growth of cancer cells[7].

Many studies have demonstrated the important role of autophagy in cervical cancer, Autophagy can be used as a target for the treatment of cervical cancer. Studies have shown that Tubeimoside I (TBM), as a new lethal autophagy lysosomal inducer, can induce autophagy accumulation and may enhance the therapeutic effect of chemotherapy drugs on cervical cancer[8]. Autophagy promotes paclitaxel resistance in cervical cancer cells[9]. Autophagy plays an important role in preventing cisplatin induced apoptosis of cervical cancer cells, so inhibition of autophagy may improve cisplatin chemotherapy[10]. However, all the above studies have revealed the role of autophagy in the occurrence and development of cervical cancer and its relationship with various tumor drugs, while few studies have studied the prognostic role of autophagy in cervical cancer.

In this study, we built a seven autophagy genes of risk model used to predict prognosis of cervical cancer oerall surial in the TCGA queue, and is verified in GES52903 queue, all have very good diagnostic performance, and further reveals the relationship between high and low risk and immune infiltration and high-risk biological function prognosis.

2 MATERIALS AND METHODS

2.1Data set selection

We downloaded the mRNA expression profiles and clinical information of cervical cancer patients from the TCGA and GEO databases, respectively, and deleted the samples with incomplete clinical information and gene expression values below 0. Since there are fewer normal cervical cancer samples in the TCGA database, there are only three cases. So We downloaded the expression values of the normal cervix from the UCSC Xena database(https://xenabrowser.net). The GSE52903 data set includes 17 normal tissues and 55 tumor tissues. The clinical information of the two data sets is shown in table 1. The list of 232 autophagy genes comes from HADb (human Bite database, http://www.autophagy.lu/)

2.2 Identify differentially expressed ARGs

We used the Wilcoxon test to analyze the difference of 232 autophagy genes based on the limma package[11], We used the Wilcoxon test to analyze the difference of 232 autophagy genes based on the limma package. The cut-off value was selected as log2 fold change (FC) > 1 and adjusted P value of < 0.05

Preprints (www.preprints.org) | NOT PEER-REVIEWED | Posted: 21 August 2020 doi:10.20944/preprints202008.0476.v1

2.3 Enrichment analysis based on univariate COX analysis of differential ARGs

In order to study the function of the differential univariate COX autophagy gene, we used the "clusterProfiler" package[12] to visualize the gene ontology (molecular function, cellular composition, biological function) and the KEGG pathway.

2.4 Genotyping of differential COX autophagy

Then we use the "ConsensusClusterPlus"[13] package to cluster the differential COX genes, use the "survival" package to see the survival curve of the typing, and use the "heatmap" package to visualize the relationship between the autophagy gene and each clinical feature. Finally, the "ggplot2[14]" package Demonstrate the relationship between different clinical features and typing.

2.5 Construction and verification of prognostic autophagy gene signatures

We identified the autophagy genes associated with the prognosis of cervical cancer by univariate Cox regression, LASSO regression and multivariate Cox regression.In summary, univariate COX regression identified the genes associated with prognosis, followed by further reduction of the genes using LASSO, multivariate COX regression。Then we constructed a risk model with the final prognostic autophagy gene, and the risk score was calculated as follows:

Risk score = $\sum_{i=1}^{n}$ Coefi × xi

Where coef is the coefficient and x is the expression level of the autophagy gene.Using this risk score, we were able to divide 261 cervical cancer patients with complete clinical data from the TCGA training set and 46 cervical cancer patients with complete clinical information from the GSE52903 validation set into high and low risk groups, We then looked at whether there were differences between the high and low risk groups in TCGA and in the clinical subtypes of GEO, The Kaplan-Meier curve was used to observe the prognosis of the high - and low-risk groups, and the receiver operating Characteristic (ROC) curve was used to assess the specificity and sensitivity of the prognostic model. Finally, the differences in clinical subtypes between high and low risk groups were demonstrated in TCGA and GEO.

2.6 Build Nomogram

Nomogram, also known as Nomogram, is a graphical method of evaluating complex functions. In this study, a nomogram was constructed using risk scores and clinical features to assess patient survival, This method visually represents the value range of different variables and their contribution to the value of risk. It is much more intuitive than simply putting a table of coefficients. The accuracy of the model was then evaluated using standard curves and combined clinical characteristic indicators (ROC).

2,7 Relationship between risk score and autophagy related genes and immunity

The immune gene set, consisting of 78 2 genes, was used to predict the abundance of 28 immune cells in 305 cervical cancer tumor tissues based on ssGESA method and implemented with GSVA R package , Immune genetic set from https://www.cell.com/cms/10.1016/j.celrep.2016.12.019/attachment/f353dac9-4bf5-4a52-bb9a-775e74d5e968/mmc3.xlsx[15], Then we looked to see whether there was a statistical difference between the 28 immune cells in the high-low risk group, and calculated the correlation between prognostic autophagy genes and 28 immune cells, and selected the cell types with $p < 0.05$ and visualized with ggplot2R package.

2.8 Draw the DCA decision curve

Stdca. R[16] was used to draw the DCA decision curve based on COX model to evaluate the clinical utility of the model

2.9 Biological function of high and low risk groups

Pi R package(http://pi314.r-forge.r-project.org/) based on the GSEA method was used to assess high and low risk group, in which biological function of enrichment of MsigdbH gene set from https://www.gsea-msigdb.org/gsea/index.jsp

2.10 Statistical Analysis

All statistical analysis is based on R software (version 3.6.3), Wilcox test was used for the difference of autophagy gene between tumor and normal tissue, and Wilcox test and Kruskal-Wallis test were used for the correlation between high and low risk score and clinical subtypes of TCGA test set and GEO verification set, The correlation between autophagy gene and immune cells was spearman method. $P < 0.05$ was considered statistically significant

3 RESULTS

3.1 Identification of ARGs

A total of 84 different autophagy genes were found in tumor tissues and normal tissues (combined with GTEX), including 44 up-regulated and 40 down-regulated genes(Figure1A and Figure1B)

3.2 Functional annotation of prognostic autophagy genes

The differential autophagy genes obtained 18 genes through the univariate COX regression method. Gene ontology enrichment analysis showed that 18 genes were mainly enriched in autophagy, macroautophagy, neuron apoptotic process, neuron death, process utilizing autophagic mechanism（Figure2A）. KEGG pathway enrichment analysis showed that these genes are mainly (Figure2B).

3.3 Identification of cervical cancer subtypes based on prognostic autophagy genes

SigClust analysis results showed that, among all the clusters, the curve was flat when consensus cluster (K = 6) (Figure 3A). Meanwhile, 261 tumor samples were divided into six molecular subtypes (Figure 3B).Survival analysis showed that subtype C4 had better survival rate than others ($P < 0.001$) (Figure 3C), The heat map shows the relationship between the expression of 18 autophagy genes and 6 subtypes and various clinical characteristics (Figure 4A), With age as the median, it could be seen that in the C2 subtype, the proportion greater than 46 years old is the smallest（Figure4B）, Subtype C1 had the highest percentage of pharmaceutical(Figure4C), In the race, White had the highest proportion among all subtypes, There are only ASIAN and WHITE in subtype C6(Figure4D), In the subtype C2, the highest proportion followed by radiotherapy(Figure4E), In subtype C5, the proportion without distant metastasis was the most, and in subtype C6, the proportion with distant metastasis was more than that of other subtypes(Figure4F), In terms of regional lymph node involvement, similar results were found with or without distant metastasis. In subtype C5, the proportion of no lymph node involvement was the highest compared with other subtypes, while in subtype C6, the proportion of a few lymph nodes involvement was the highest(Figure4G), In terms of primary tumors, the proportion of T1 in subtype C6 was the smallest compared with other subtypes, and the proportion of T2 was the largest, and only these two types(Figure4H), In the tumor grade, the proportion of G2 in subtype C6 was the largest(Figure4I).

3.3 Construction and validation of a risk model based on 7 autophagy genes

In the training set TCGA,the 18 autophagy genes obtained by the univariate COX regression method (Figure 5A) were further reduced by the LASSO regression method (Figure 5B), and finally 7 autophagy genes (Table2)were used for the construction of the risk signature based on the multivariate COX regression method (Figure5C). risk score =0.466*(expression level of

 doi:10.20944/preprints202008.0476.v1

HGS)+0.432*(expression level of GAPDH)+(-0.447)*(expression level of ATG4A)+(-0.482)*(expression level of BCL2)+0.862*(expression level of TM9SF1)+1.329*(expression level of ATF6)+0.573*(expression level of NCKAP1). We then calculated each patient's risk score and divided them into high and low risk groups according to the median of the scores in the TCGA cohort of the training set (Figure 6A) and the GES52902 cohort of the verification set (Figure 6B), The patient's survival status, survival time and autophagy gene expression were shown in Figure 6A (TCGA) and Figure 6B(GSE52903), As can be seen from the graph, the number of patients dying gradually increased as the risk score increased, Survival analysis showed that the high-risk group had a worse prognosis in TCGA ($P < 0.0001$) (Figure 7A), with a consistent result $p < 0.05$ in the GES52903 validation set (Figure 7B). ROC curve analysis results show that the AUC value in TCGA was 0.894 (Figure 7C), in GES52903, the AUC value was 0.736 (Figure 7D), and the AUC values for 1, 3, and 5 years were 0.78, 0.77, 0.81, and 0.82, respectively , 0.72, 0.72, suggesting that the risk score had a good predictive ability for overall survival.

3.4 Relationship between risk score and clinical traits

As shown in Figure 8, the risk score in the TCGA cohort showed statistically significant differences in tumor grade, metastasis, lymph node involvement, and T stage, while in the GSE52903 cohort, there was no difference in age and stage, and in the TCGA cohort, age, whether the patient had received pharmaceutical or radiotherapy, was not significant, It suggests that risk score is closely related to TMN of tumor.

3,5 Construction of nomogram

Based on the risk score, age, G, T, M, and N staging nomograph was constructed (Figure 9A). From the figure, it can be drawn that the total score based on the above indicators can be predicted for each patient for 1 year, 2 Year, 3 year survival rate.

The standard curve was used to evaluate the predictive ability of the Nomograph. As shown in Figure 9B, the 1-year, 2-year, and 3-year curve levels overlap well with the standard curve. At the same time, the multi-index ROC curve analysis results of combined clinical traits showed that the risk score AUC area of 1 year, 2 years, and 3 years were all higher than other clinical characteristics, which were 0.782, 0.763, and 0.783 respectively(Figure9C). The above results indicate that the risk scoring model has good predictive ability.

3.6 DCA curve drawing

Considering the clinical utility of the risk model, we drew the DCA curve. As shown in Figure 10, the model combined with the risk score was more beneficial than the model with only age and TMN staging. Figure 10A, Figure 10B, and Figure 10C respectively for one year, two years, and three years of DCA curve

3.7 Relationship between risk models constructed by 7 autophagy genes and immune cells and their biological functions

As showned in Figure 11A, high and low risk scores differed in most immune cells, except CD56bright natural killer cell, Central Memory CD8 T cell, Gamma Delta T cell, Neutrophil, Regulatory T cell, T helper cell, and Type 2 T helper cell. Figure 11B-H showed the correlation between HGS, GAPDH, ATG4A, BCL2, TM9SF1, ATF6, NCKAP1 gene and differential immune cells. Then performed GESA enrichment analysis on the high and low risk scores. As showned in Figure 12, the high-risk group was mainly enriched in the G2/M checkpoint, as in progression through the cell division cycle, Genes defining epithelial-mesenchymal transition, as in wound healing, fibrosis and metastasis. Genes up-regulated in response to low oxygen levels (hypoxia),

 doi:10.20944/preprints202008.0476.v1

Genes important for mitotic spindle assembly. These biological functions was closely related to the occurrence of tumors.

DISCUSSION

Many studies have shown that autophagy is involved in multiple signaling pathways to affect the occurrence and development of cervical cancer[17-21]. Studies have shown that inhibitors of autophagy gene ATG4 can inhibit autophagy, enhance the cytotoxicity of chemotherapy drugs, and achieve the purpose of killing tumor cells[22]. Autophagy gene BCL2 can be used as a therapeutic target of some drugs for cervical cancer[23]. TM9SF1 gene can bind to estrogen receptor, regulate the epithelial-mesenchymal transformation of cancer cells, and promote tumor metastasis[24]. ATF6 is also closely related to the occurrence of colorectal cancer[25]. NCKAP1 is involved in breast cancer metastasis[26].

In the current study, we combined the normal cervical expression profile data of GETX with the data in TCGA to extract the expression data of all autophagy genes, and obtained 84 differential autophagy genes, which were determined by single factor COX regression analysis. 18 Autophagy genes related to prognosis, and then the functional enrichment of these genes was found to be mainly enriched in autophagy, apoptosis, HIF-1 signaling pathway, etc., which are closely related to the occurrence of tumors[27,28]. At the same time, 18 genotypes were classified into 6 subtypes, and the distribution of each clinical trait in each subtype was not the same. Next, use LASSO regression and multi-factor COX regression methods to obtain the final 7 autophagy genes for use in constructing a prognosis model for cervical cancer patients. At the same time, 18 genotypes were classified into 6 subtypes, and the distribution of each clinical trait in each subtype was not the same. Next, use LASSO regression and multi-factor COX regression methods to obtain the final 7 autophagy genes for constructing a prognostic risk model for cervical cancer patients. High-risk prognosis is poor, tumors are relatively large, there are more organs involved, and there are more distant metastases and lymph node involvement. Nomo diagram is also called nomogram. Its advantage lies in transforming complex regression equations into simple visualization graphs, making the results of prognostic models readable and widely used in clinical applications[29-32]. In this study, a risk score, age, grade, and stage were constructed to predict the 1, 2, and 3 year survival probability of cervical cancer patients. And 1-, 2-, 3-year AUC values are all higher than age, classification and staging. The nomogram is prediction, so the decision curve analysis method (DCA) is to solve the clinical utility problem and solve the clinical practicality of the nomogram. Now it is also widely used in various fields, such as predicting the prognosis of lung cancer[33], sentinel lymph node metastasis of skin melanoma[34], The prognosis of left atrial enlargement in degenerative mitral regurgitation[35]. In this study, after adding the risk score signature, patients benefited more from 1-, 2-, 3-years. Immune infiltration is also a hot topic of research so far. Studies have found that the combination of immune checkpoint inhibitors and cisplatin anticancer drugs can enhance the therapeutic effect of cervical cancer[36]. In this study, the immune enrichment score of most immune cells in the high-risk group was lower than that in the low-risk group, and the immune activity of the high-risk group was suppressed, which is more conducive to the proliferation of tumor cells. GSEA enrichment analysis results show that the high-risk group is mainly enriched at the G2/M checkpoint, such as the process through the cell division cycle; genes that define epithelia1-mesenchymal transition, such as wound healing, fibrosis and metastasis. Genes that are up-regulated in response to low oxygen levels (hypoxia) are genes that are important for mitotic spindle assembly. The cell division cycle is directly inseparable from the proliferation of tumor cells.

Studies have shown that hypoxia is related to the poor prognosis of tumor patients[37]. EMT provides a channel for tumor cell metastasis[38]. These biological functions can lead to poor prognosis and more deaths in high-risk groups.

In short, the seven autophagy prognostic signatures that we have constructed may become prognostic tools for cervical cancer, whether in prediction or clinical application, and can be used as personalized treatment strategies for cervical cancer patients.

AUTHOR CONTRIBUTIONS

J.Q.J., and H.L.,designed the study and conceived the project. H.Y.X., P.S.Z.,performed the experiments and analyzed the data.H.L. drafted the manuscript.

DISCLOSURE

The authors report no conflicts of interest in this work.

References:

1. Cohen, P.A.; Jhingran, A.; Oaknin, A.; Denny, L., Cervical cancer. *LANCET* **2019**, 393, (10167), 169-182.
2. Bray, F.; Ferlay, J.; Soerjomataram, I.; Siegel, R.L.; Torre, L.A.; Jemal, A., Global cancer statistics 2018: GLOBOCAN estimates of incidence and mortality worldwide for 36 cancers in 185 countries. *CA Cancer J Clin* **2018**, 68, (6), 394-424.
3. Meijer, C.; Steenbergen, R., Gynaecological cancer: Novel molecular subtypes of cervical cancer - potential clinical consequences. *NAT REV CLIN ONCOL* **2017**, 14, (7), 397-398.
4. Allaire, M.; Rautou, P.E.; Codogno, P.; Lotersztajn, S., Autophagy in liver diseases: Time for translation? *J HEPATOL* **2019**, 70, (5), 985-998.
5. Lopez-Otin, C.; Kroemer, G., Decelerating ageing and biological clocks by autophagy. *Nat Rev Mol Cell Biol* **2019**, 20, (7), 385-386.
6. Venida, A.; Perera, R.M., Host Control of Tumor Feeding: Autophagy Holds the Key. *CELL METAB* **2019**, 29, (2), 236-238.
7. Harjes, U., Maintaining the tumour's diet. *NAT REV CANCER* **2019**, 19, (2), 62-63.
8. Feng, X.; Zhou, J.; Li, J.; Hou, X.; Li, L.; Chen, Y.; Fu, S.; Zhou, L.; Li, C.; Lei, Y., Tubeimoside I induces accumulation of impaired autophagolysosome against cervical cancer cells by both initiating autophagy and inhibiting lysosomal function. *CELL DEATH DIS* **2018**, 9, (11), 1117.
9. Peng, X.; Gong, F.; Chen, Y.; Jiang, Y.; Liu, J.; Yu, M.; Zhang, S.; Wang, M.; Xiao, G.; Liao, H., Autophagy promotes paclitaxel resistance of cervical cancer cells: involvement of Warburg effect activated hypoxia-induced factor 1-alpha-mediated signaling. *CELL DEATH DIS* **2014**, 5, e1367.
10. Xu, Y.; Yu, H.; Qin, H.; Kang, J.; Yu, C.; Zhong, J.; Su, J.; Li, H.; Sun, L., Inhibition of autophagy enhances cisplatin cytotoxicity through endoplasmic reticulum stress in human cervical cancer cells. *CANCER LETT* **2012**, 314, (2), 232-43.
11. Ritchie, M.E.; Phipson, B.; Wu, D.; Hu, Y.; Law, C.W.; Shi, W.; Smyth, G.K., limma powers differential expression analyses for RNA-sequencing and microarray studies. *NUCLEIC ACIDS*

RES **2015**, 43, (7), e47.

12. Yu, G.; Wang, L.G.; Han, Y.; He, Q.Y., clusterProfiler: an R package for comparing biological themes among gene clusters. *OMICS* **2012**, 16, (5), 284-7.
13. Wilkerson, M.D.; Hayes, D.N., ConsensusClusterPlus: a class discovery tool with confidence assessments and item tracking. *BIOINFORMATICS* **2010**, 26, (12), 1572-3.
14. Ito, K.; Murphy, D., Application of ggplot2 to Pharmacometric Graphics. *CPT Pharmacometrics Syst Pharmacol* **2013**, 2, e79.
15. Charoentong, P.; Finotello, F.; Angelova, M.; Mayer, C.; Efremova, M.; Rieder, D.; Hackl, H.; Trajanoski, Z., Pan-cancer Immunogenomic Analyses Reveal Genotype-Immunophenotype Relationships and Predictors of Response to Checkpoint Blockade. *CELL REP* **2017**, 18, (1), 248-262.
16. Vickers, A.J.; Cronin, A.M., Traditional statistical methods for evaluating prediction models are uninformative as to clinical value: towards a decision analytic framework. *SEMIN ONCOL* **2010**, 37, (1), 31-8.
17. Wu, G.; Long, Y.; Lu, Y.; Feng, Y.; Yang, X.; Xu, X.; Yao, D., Kindlin2 suppresses cervical cancer cell migration through AKT/mTORmediated autophagy induction. *ONCOL REP* **2020**, 44, (1), 69-76.
18. Liu, F.; Chang, L.; Hu, J., Activating transcription factor 6 regulated cell growth, migration and inhibiteds cell apoptosis and autophagy via MAPK pathway in cervical cancer. *J REPROD IMMUNOL* **2020**, 139, 103120.
19. Xiang, W.; Zhang, R.J.; Jin, G.L.; Tian, L.; Cheng, F.; Wang, J.Z.; Xing, X.F.; Xi, W.; Tang, S.J.; Chen, J.F., RCE4, a potential anticervical cancer drug isolated from Reineckia carnea, induces autophagy via the dual blockade of PI3K and ERK pathways in cervical cancer CaSki cells. *INT J MOL MED* **2020**, 45, (1), 245-254.
20. Guo, X.; Xiao, H.; Guo, S.; Li, J.; Wang, Y.; Chen, J.; Lou, G., Long noncoding RNA HOTAIR knockdown inhibits autophagy and epithelial-mesenchymal transition through the Wnt signaling pathway in radioresistant human cervical cancer HeLa cells. *J CELL PHYSIOL* **2019**, 234, (4), 3478-3489.
21. Lu, R.; Yang, Z.; Xu, G.; Yu, S., miR-338 modulates proliferation and autophagy by PI3K/AKT/mTOR signaling pathway in cervical cancer. *BIOMED PHARMACOTHER* **2018**, 105, 633-644.
22. Liu, P.F.; Tsai, K.L.; Hsu, C.J.; Tsai, W.L.; Cheng, J.S.; Chang, H.W.; Shiau, C.W.; Goan, Y.G.; Tseng, H.H.; Wu, C.H.; Reed, J.C.; Yang, L.W.; Shu, C.W., Drug Repurposing Screening Identifies Tioconazole as an ATG4 Inhibitor that Suppresses Autophagy and Sensitizes Cancer Cells to Chemotherapy. *THERANOSTICS* **2018**, 8, (3), 830-845.
23. Wang, X.; Yi, Y.; Lv, Q.; Zhang, J.; Wu, K.; Wu, W.; Zhang, W., Novel 1,3,5-triazine derivatives exert potent anti-cervical cancer effects by modulating Bax, Bcl2 and Caspases expression. *CHEM BIOL DRUG DES* **2018**, 91, (3), 728-734.
24. Miyazaki, T.; Ikeda, K.; Sato, W.; Horie-Inoue, K.; Inoue, S., Extracellular vesicle-mediated EBAG9 transfer from cancer cells to tumor microenvironment promotes immune escape and tumor progression. *ONCOGENESIS* **2018**, 7, (1), 7.
25. Lavoie, S.; Garrett, W.S., The Unfolding Story of ATF6, Microbial Dysbiosis, and Colorectal Cancer. *GASTROENTEROLOGY* **2018**, 155, (5), 1309-1311.
26. Teng, Y.; Qin, H.; Bahassan, A.; Bendzunas, N.G.; Kennedy, E.J.; Cowell, J.K., The WASF3-

NCKAP1-CYFIP1 Complex Is Essential for Breast Cancer Metastasis. *CANCER RES* **2016**, 76, (17), 5133-42.

27. Carneiro, B.A.; El-Deiry, W.S., Targeting apoptosis in cancer therapy. *NAT REV CLIN ONCOL* **2020**, 17, (7), 395-417.
28. LaGory, E.L.; Giaccia, A.J., The ever-expanding role of HIF in tumour and stromal biology. *NAT CELL BIOL* **2016**, 18, (4), 356-65.
29. Xu, L.; Peng, Z.W.; Chen, M.S.; Shi, M.; Zhang, Y.J.; Guo, R.P.; Lin, X.J.; Lau, W.Y., Prognostic nomogram for patients with unresectable hepatocellular carcinoma after transcatheter arterial chemoembolization. *J HEPATOL* **2015**, 63, (1), 122-30.
30. Liang, W.; Zhang, L.; Jiang, G.; Wang, Q.; Liu, L.; Liu, D.; Wang, Z.; Zhu, Z.; Deng, Q.; Xiong, X.; Shao, W.; Shi, X.; He, J., Development and validation of a nomogram for predicting survival in patients with resected non-small-cell lung cancer. *J CLIN ONCOL* **2015**, 33, (8), 861-9.
31. Wang, Y.; Li, J.; Xia, Y.; Gong, R.; Wang, K.; Yan, Z.; Wan, X.; Liu, G.; Wu, D.; Shi, L.; Lau, W.; Wu, M.; Shen, F., Prognostic nomogram for intrahepatic cholangiocarcinoma after partial hepatectomy. *J CLIN ONCOL* **2013**, 31, (9), 1188-95.
32. Lo, S.N.; Ma, J.; Scolyer, R.A.; Haydu, L.E.; Stretch, J.R.; Saw, R.; Nieweg, O.E.; Shannon, K.F.; Spillane, A.J.; Ch'Ng, S.; Mann, G.J.; Gershenwald, J.E.; Thompson, J.F.; Varey, A., Improved Risk Prediction Calculator for Sentinel Node Positivity in Patients With Melanoma: The Melanoma Institute Australia Nomogram. *J CLIN ONCOL* **2020**, JCO1902362.
33. Burki, T.K., Predicting lung cancer prognosis using machine learning. *LANCET ONCOL* **2016**, 17, (10), e421.
34. Maurichi, A.; Miceli, R.; Eriksson, H.; Newton-Bishop, J.; Nsengimana, J.; Chan, M.; Hayes, A.J.; Heelan, K.; Adams, D.; Patuzzo, R.; Barretta, F.; Gallino, G.; Harwood, C.; Bergamaschi, D.; Bennett, D.; Lasithiotakis, K.; Ghiorzo, P.; Dalmasso, B.; Manganoni, A.; Consoli, F.; Mattavelli, I.; Barbieri, C.; Leva, A.; Cortinovis, U.; Espeli, V.; Mangas, C.; Quaglino, P.; Ribero, S.; Broganelli, P.; Pellacani, G.; Longo, C.; Del, F.C.; Borgognoni, L.; Sestini, S.; Pimpinelli, N.; Fortunato, S.; Chiarugi, A.; Nardini, P.; Morittu, E.; Florita, A.; Cossa, M.; Valeri, B.; Milione, M.; Pruneri, G.; Zoras, O.; Anichini, A.; Mortarini, R.; Santinami, M., Factors Affecting Sentinel Node Metastasis in Thin (T1) Cutaneous Melanomas: Development and External Validation of a Predictive Nomogram. *J CLIN ONCOL* **2020**, 38, (14), 1591-1601.
35. Essayagh, B.; Antoine, C.; Benfari, G.; Messika-Zeitoun, D.; Michelena, H.; Le Tourneau, T.; Mankad, S.; Tribouilloy, C.M.; Thapa, P.; Enriquez-Sarano, M., Prognostic Implications of Left Atrial Enlargement in Degenerative Mitral Regurgitation. *J AM COLL CARDIOL* **2019**, 74, (7), 858-870.
36. Wang, N.; Wang, Z.; Xu, Z.; Chen, X.; Zhu, G., A Cisplatin-Loaded Immunochemotherapeutic Nanohybrid Bearing Immune Checkpoint Inhibitors for Enhanced Cervical Cancer Therapy. *Angew Chem Int Ed Engl* **2018**, 57, (13), 3426-3430.
37. Jing, X.; Yang, F.; Shao, C.; Wei, K.; Xie, M.; Shen, H.; Shu, Y., Role of hypoxia in cancer therapy by regulating the tumor microenvironment. *MOL CANCER* **2019**, 18, (1), 157.
38. Dongre, A.; Weinberg, R.A., New insights into the mechanisms of epithelial-mesenchymal transition and implications for cancer. *Nat Rev Mol Cell Biol* **2019**, 20, (2), 69-84.

Preprints (www.preprints.org) | NOT PEER-REVIEWED | Posted: 21 August 2020 doi:10.20944/preprints202008.0476.v1

Table1 Clinical information of cervical cancer patients in the TCGA cohort and the GSE52903 cohort

TCGA

	alive (N=197)	dead (N=64)
age		
age > 47	88 (44.7%)	34 (53.1%)
age<=47	109 (55.3%)	30 (46.9%)
race		
AMERICAN INDIAN OR ALASKA NATIVE	4 (2.0%)	3 (4.7%)
ASIAN	17 (8.6%)	4 (6.2%)
BLACK OR AFRICAN AMERICAN	20 (10.2%)	8 (12.5%)
WHITE	156 (79.2%)	49 (76.6%)
radiation		
NO	72 (36.5%)	15 (23.4%)
YES	125 (63.5%)	49 (76.6%)
pharmaceutical		
NO	95 (48.2%)	24 (37.5%)
YES	102 (51.8%)	40 (62.5%)
tumor_grade		
G1	15 (7.6%)	1 (1.6%)
G2	83 (42.1%)	35 (54.7%)
G3	87 (44.2%)	22 (34.4%)
G4	12 (6.1%)	6 (9.4%)
stage_T		
T1a1	1 (0.5%)	0 (0%)
T1b	37 (18.8%)	10 (15.6%)
T1b1	60 (30.5%)	17 (26.6%)
T1b2	27 (13.7%)	9 (14.1%)

Preprints (www.preprints.org) | NOT PEER-REVIEWED | Posted: 21 August 2020 doi:10.20944/preprints202008.0476.v1

T2	5 (2.5%)	3 (4.7%)
T2a	10 (5.1%)	3 (4.7%)
T2a1	7 (3.6%)	0 (0%)
T2a2	11 (5.6%)	1 (1.6%)
T2b	25 (12.7%)	8 (12.5%)
T3	2 (1.0%)	0 (0%)
T3a	2 (1.0%)	0 (0%)
T3b	7 (3.6%)	6 (9.4%)
T4	3 (1.5%)	7 (10.9%)
stage_M		
M0	94 (47.7%)	22 (34.4%)
M1	5 (2.5%)	3 (4.7%)
MX	98 (49.7%)	39 (60.9%)
stage_N		
N0	124 (62.9%)	26 (40.6%)
N1	39 (19.8%)	21 (32.8%)
NX	34 (17.3%)	17 (26.6%)

GSE52903

	alive (N=28)	**dead (N=18)**
Age (yeas)		
age > 49	14 (50.0%)	9 (50.0%)
age<=49	14 (50.0%)	9 (50.0%)
stage		
IB1	14 (50.0%)	1 (5.6%)
IB2	6 (21.4%)	3 (16.7%)
IIA	1 (3.6%)	1 (5.6%)
IIB	3 (10.7%)	2 (11.1%)
IIIB	4 (14.3%)	8 (44.4%)
IVA	0 (0%)	1 (5.6%)
IVB	0 (0%)	2 (11.1%)

Preprints (www.preprints.org) | NOT PEER-REVIEWED | Posted: 21 August 2020 doi:10.20944/preprints202008.0476.v1

Table2 Independent autophagy genes in signatures

id	coef	HR	HR.95L	HR.95H	pvalue
HGS	0.465969773	1.59355883	0.845394965	3.003838267	0.149672212
GAPDH	0.431521264	1.539597878	1.04154736	2.27580782	0.030455504
ATG4A	−0.447145542	0.639450834	0.345371503	1.183934883	0.154813021
BCL2	−0.482115456	0.617475766	0.377809895	1.009175057	0.054414196
TM9SF1	0.862421717	2.368890535	1.029297726	5.451913695	0.04257417
ATF6	1.329063414	3.777503775	1.468861276	9.71469192	0.005819841
NCKAP1	0.573031525	1.773635731	0.936920157	3.35757928	0.078431993

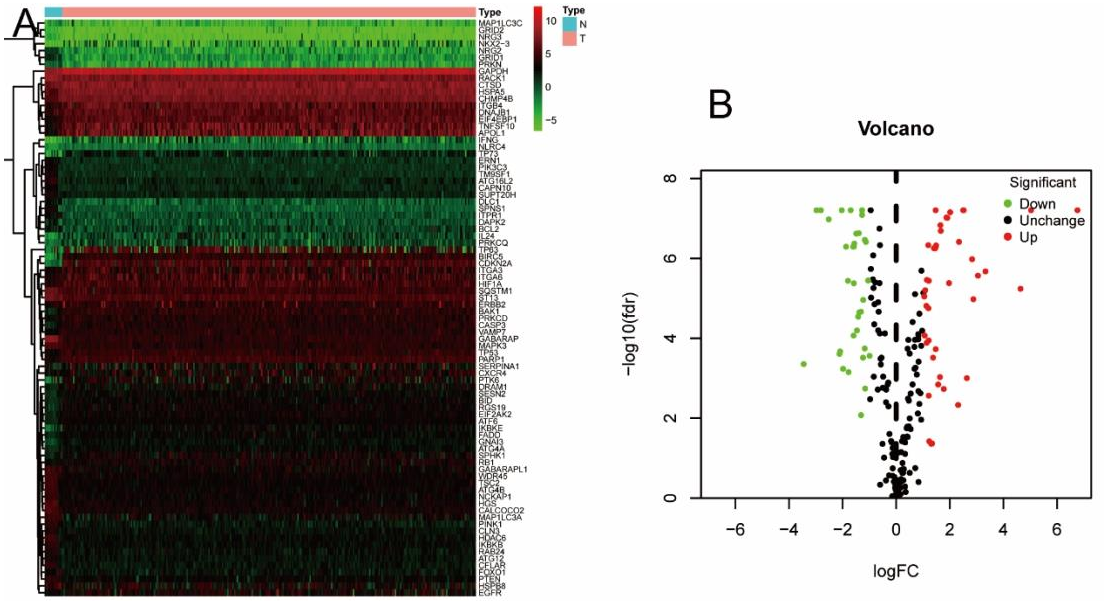

Figure 1: Identify differentially expressed autophagy genes. (A): Heatmap of differential autophagy genes in cervical cancer. (B): Volcano map of differential autophagy genes, Absolute log2-fold change (FC) > 1 and adjusted P value <0.05 were used as screening criteria for differential genes.

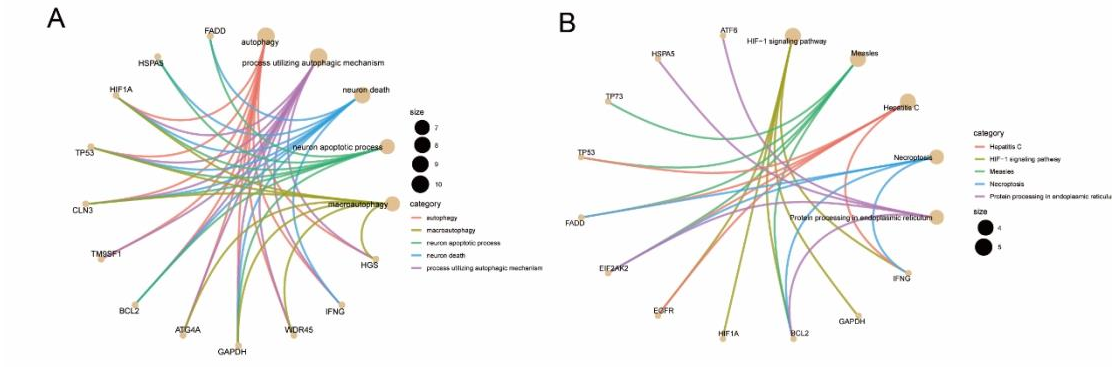

Figure 2: Functional enrichment of prognostic autophagy genes. (A): Analysis of the top five most

Preprints (www.preprints.org) | NOT PEER-REVIEWED | Posted: 21 August 2020 doi:10.20944/preprints202008.0476.v1

important gene ontology. (B): Analysis of the top five most important KEGG pathways.

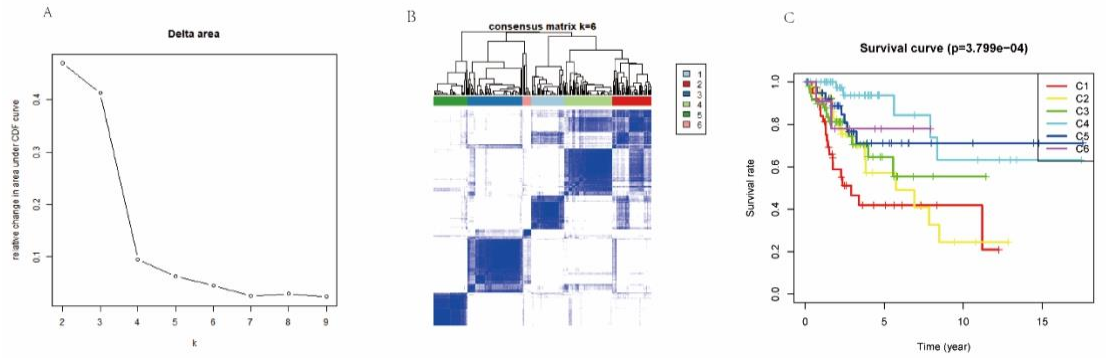

Figure 3: Prognostic autophagy genotyping and genotyping survival analysis. (A): CDF Delta area curves for all samples. (B): When K = 6 (1 = C1, 2 = C2, 3 = C3, 4 = C4, 5 = C5, 6=C6), cervical cancer patients were divided into subtype matrix. (C): Survival curve analysis of 6 subtypes.

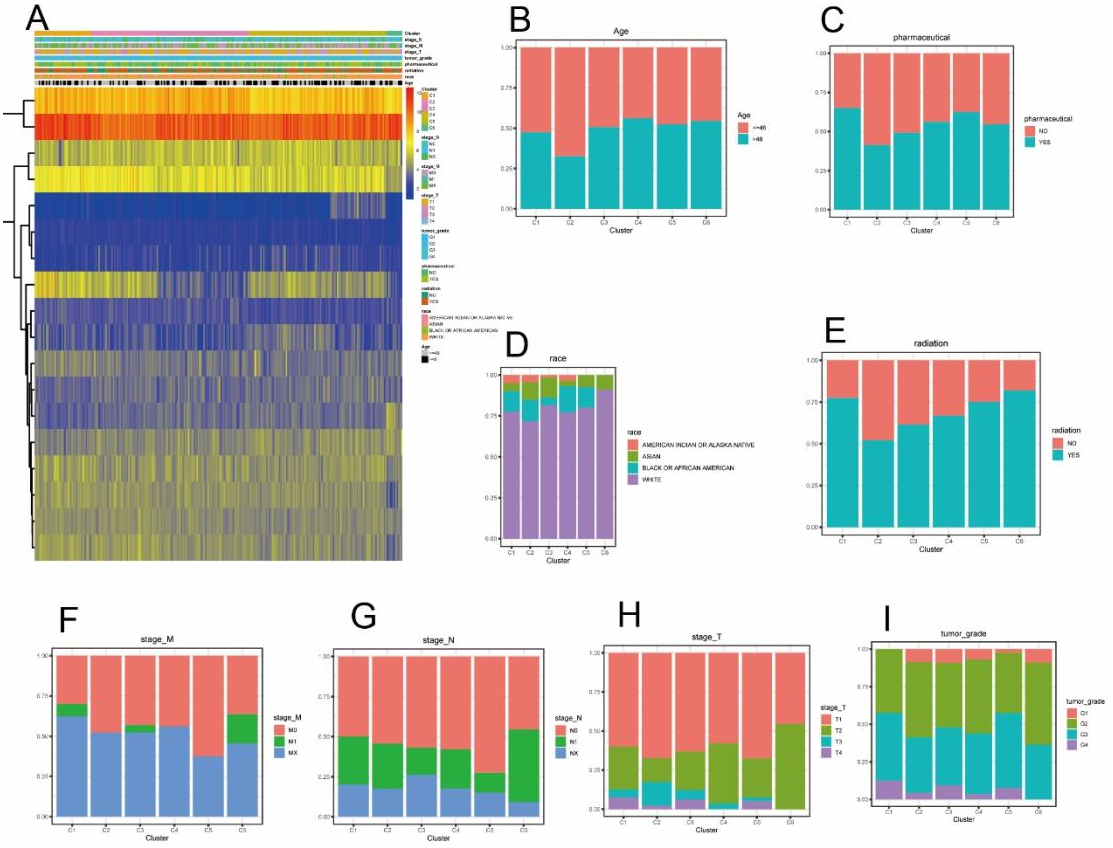

Figure 4: Correlation between 6 subtypes and clinical characteristics. (A): The heat map shows the expression values, subtypes and clinical characteristics of 18 autophagy genes. Red indicates high expression and blue indicates low expression. (B): Distribution of age in subtypes. (C): Distribution of pharmaceutical treatments among subtypes. (D): Distribution of different races in subtypes. (E): Distribution of radiation therapy in subtypes. (F): Distribution of M stages in subtypes. (G): Distribution of N stages in subtypes. (H): Distribution of T stages in subtypes. (I): Distribution of Grade in subtypes.

Preprints (www.preprints.org) | NOT PEER-REVIEWED | Posted: 21 August 2020 doi:10.20944/preprints202008.0476.v1

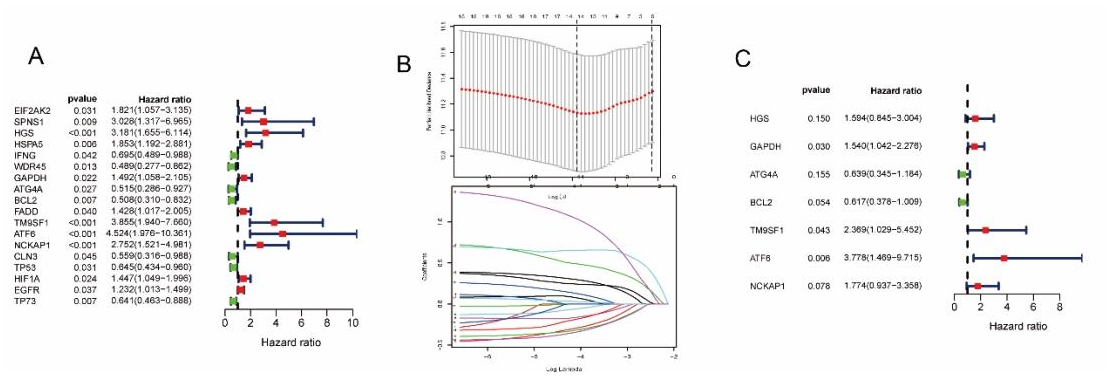

Figure5: Identification of 7 autophagy prognostic genes. (A): Univariate COX regression analysis of differential autophagy genes. (B): Lasso regression analysis of 17 autophagy genes. (C): Multivariate COX regression analysis of autophagy genes.

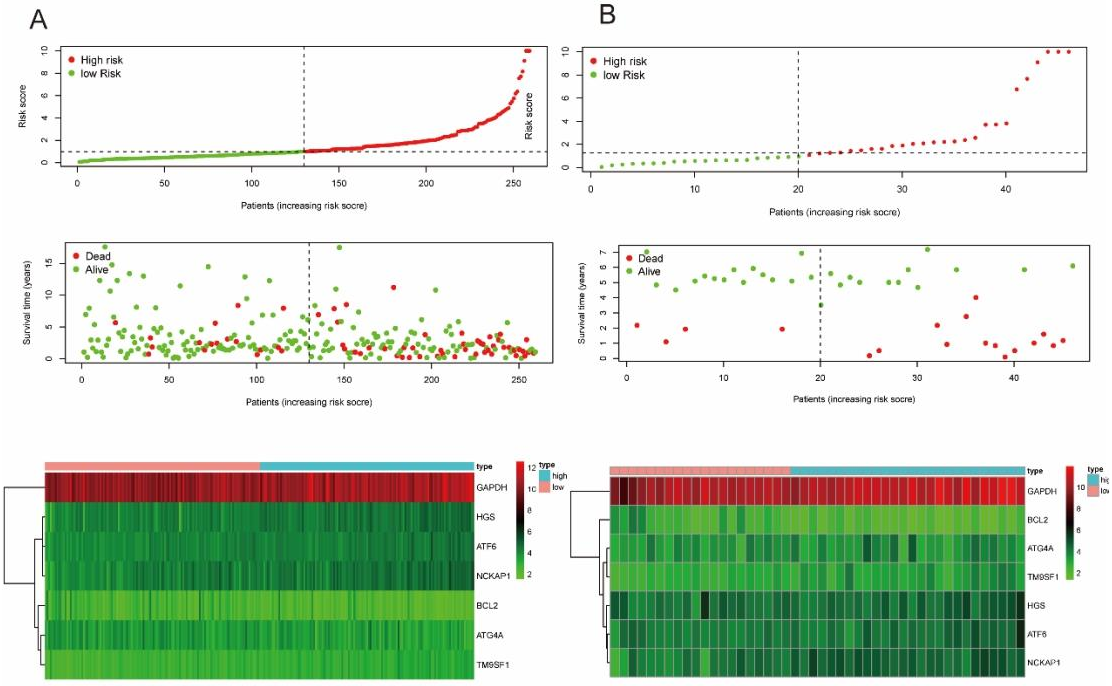

Figure6: Construction and validation of risk signatures of 7 autophagy prognostic genes. (A-B): The relationship between risk score (top), risk score and survival time (middle), risk score and gene expression in training set TCGA (A) and validation set GSE52903 (B). The black dotted line represents the median of the risk score.

Preprints (www.preprints.org) | NOT PEER-REVIEWED | Posted: 21 August 2020 doi:10.20944/preprints202008.0476.v1

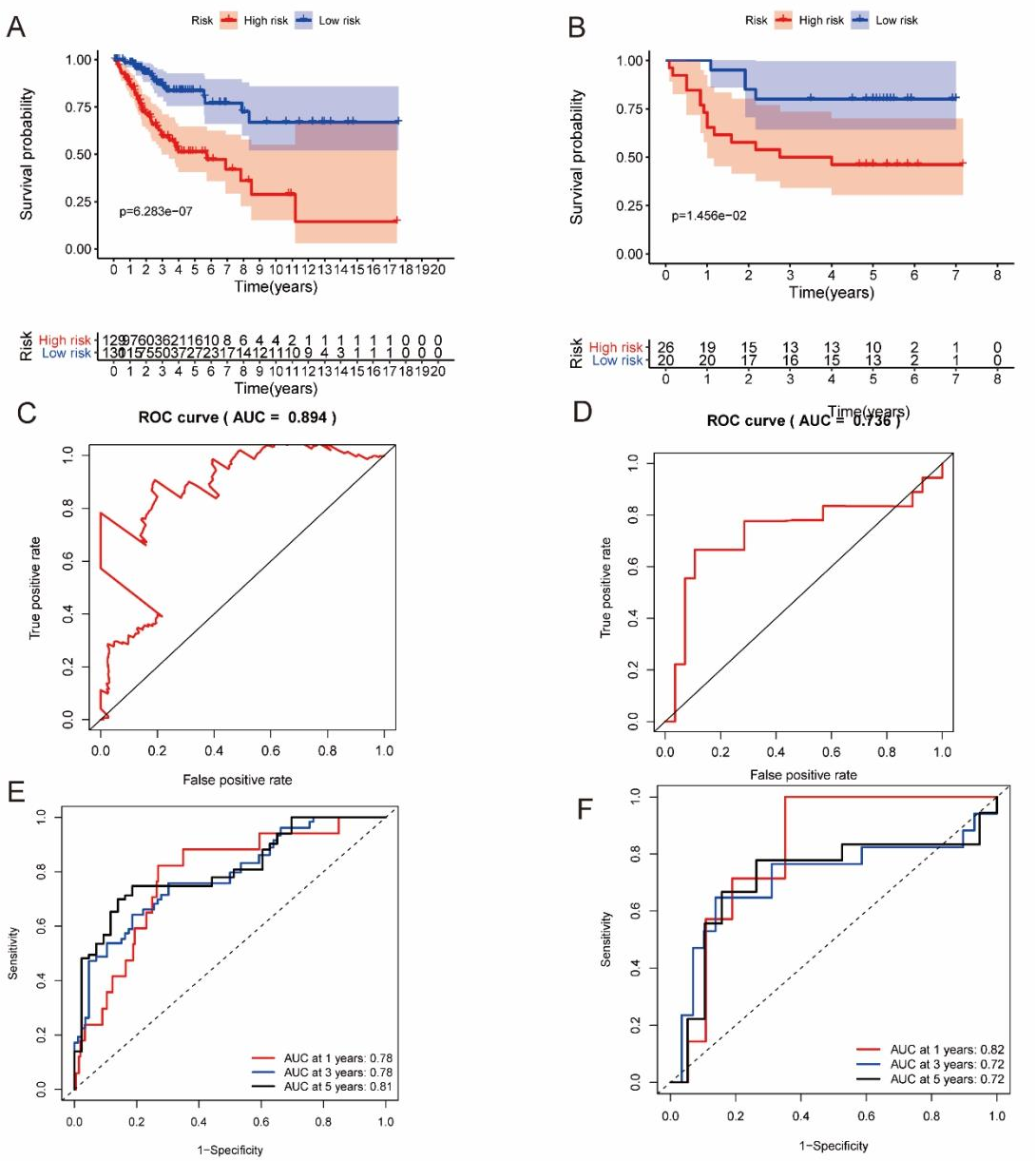

Figure7: Kaplan-meier survival analysis and ROC curve analysis risk model. (A-B): Kaplan-meier survival curves of the high and low risk groups were found in TCGA(A) and GSE52903(B). (C-D):ROC curve analysis in TCGA(C) and GSE52903(D). (E-F):The ROC curve analysis used to predict 1 year, 3 years, and 5 years is in TCGA(E) and GSE52903(F).

Preprints (www.preprints.org) | NOT PEER-REVIEWED | Posted: 21 August 2020 doi:10.20944/preprints202008.0476.v1

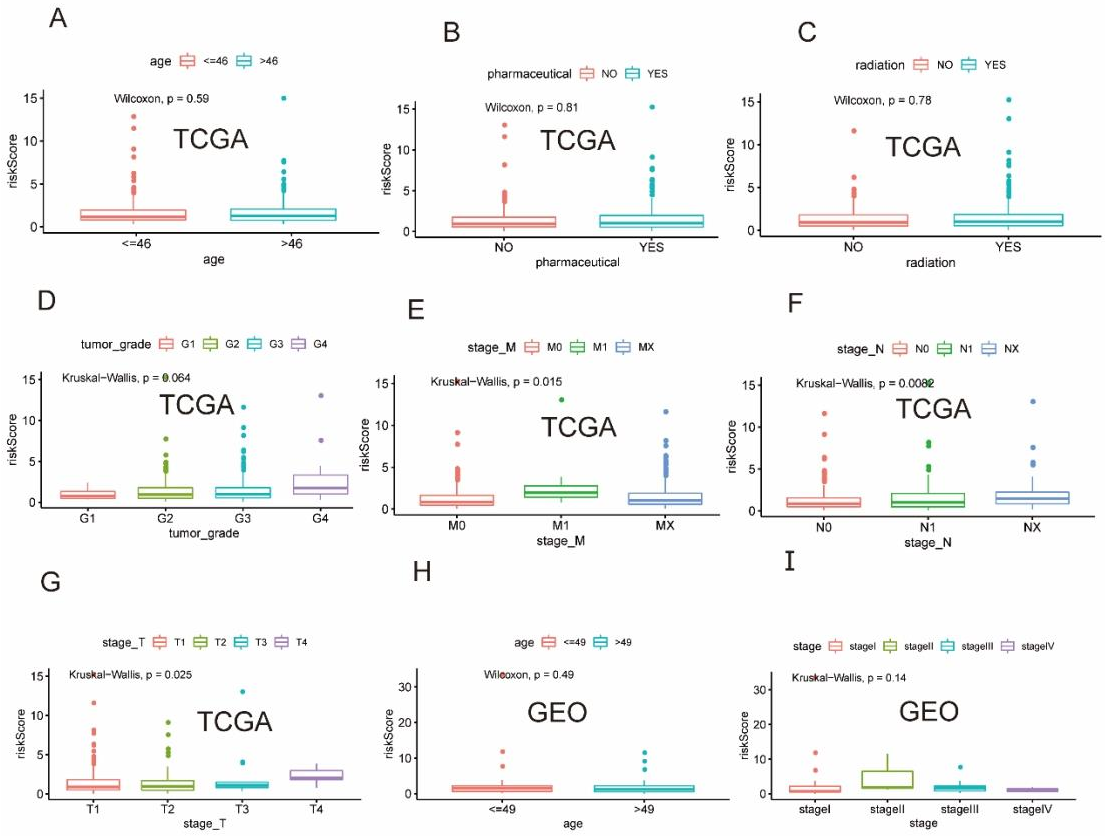

Figure8: Differences in risk scores of various clinical traits. (A): In TCGA, the difference in risk scores with age as the median value,p=0.59. (B): Differences in risk scores in the pharmaceutical in TCGA ,p=0.81. (C): Difference in risk score between receiving radiation therapy and not receiving radiation therapy in TCGA.p=0.78. (D): Risk scores differed among different grading groups in TCGA .p=0.064. (E): Differences between different M staging groups in TCGA.p=0.015. (F): Differences between different N staging groups in TCGA.p=0.0082. (G): Differences between different T staging groups in TCGA .p=0.025. (H): Difference in risk scores with age as the median value in GES52903,p=0.49. (I): Differences between staging groups in GSE52903,p=0.14.

Preprints (www.preprints.org) | NOT PEER-REVIEWED | Posted: 21 August 2020 doi:10.20944/preprints202008.0476.v1

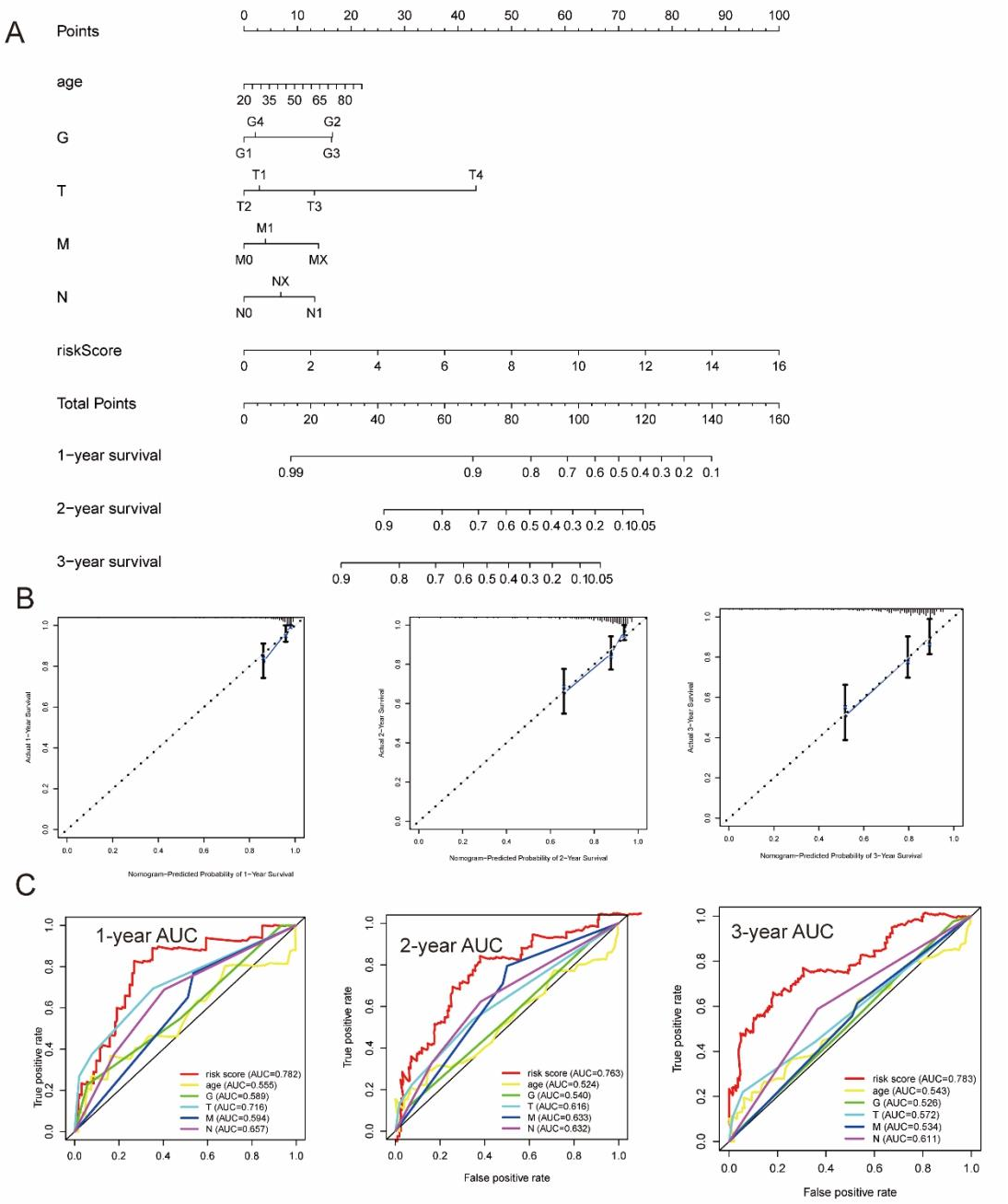

Figure9: Constructing a nomograph in cervical cancer to predict overall survival. (A): Risk score and age, G, T, M, N nomograph. (B): Standard curve for predicting 1, 2, and 3 year overall survival rate. (C): Multi-index ROC curve analysis of risk score and clinical characteristics.

Preprints (www.preprints.org) | NOT PEER-REVIEWED | Posted: 21 August 2020 doi:10.20944/preprints202008.0476.v1

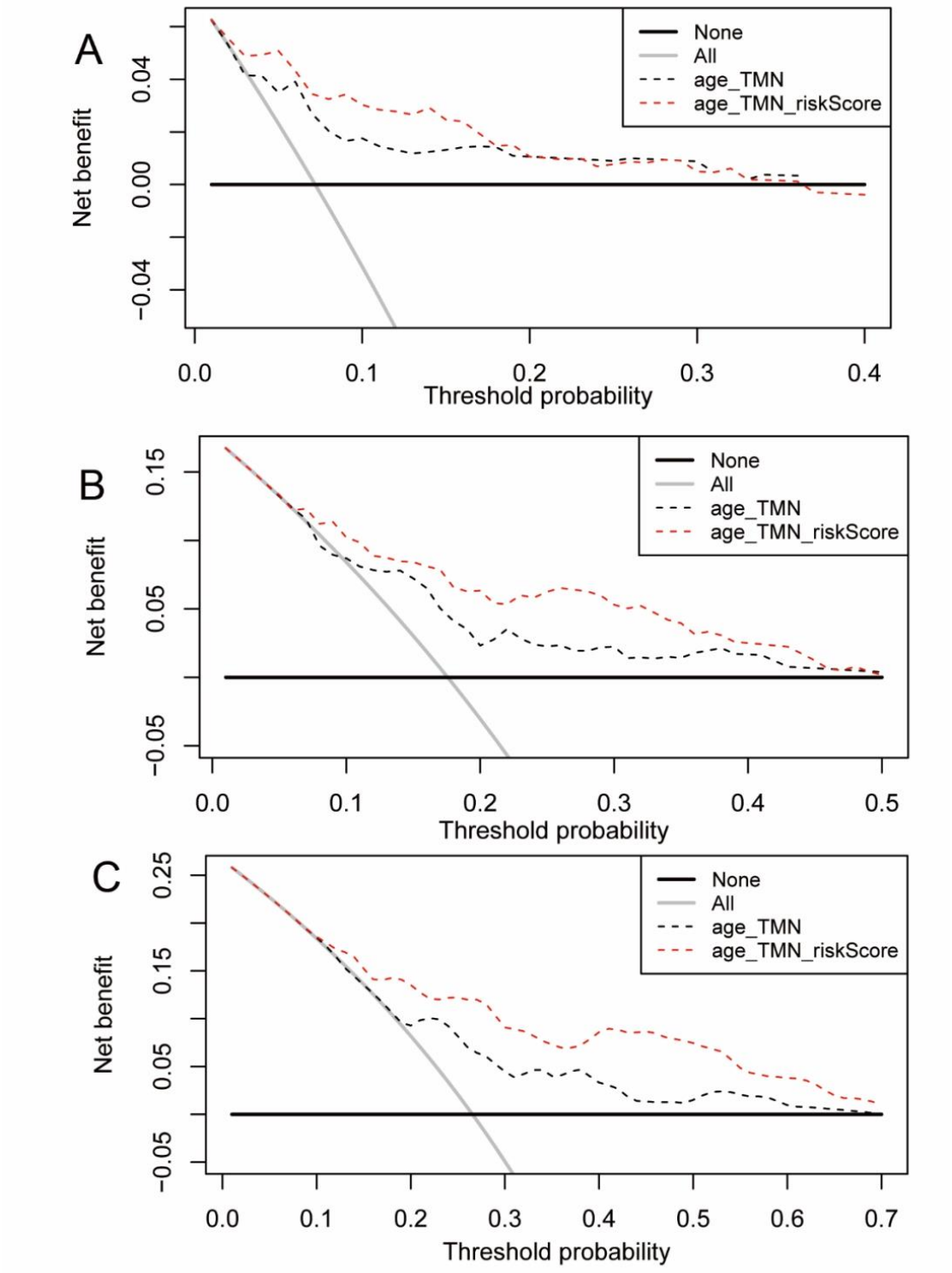

Figure10: Construct the DCA curve. (A-C): The DCA curve of a model with a joint risk score of 1 year (10A), 2 years (10B), and 3 (10C) years and a model with only age and TMN stage.

Preprints (www.preprints.org) | NOT PEER-REVIEWED | Posted: 21 August 2020 doi:10.20944/preprints202008.0476.v1

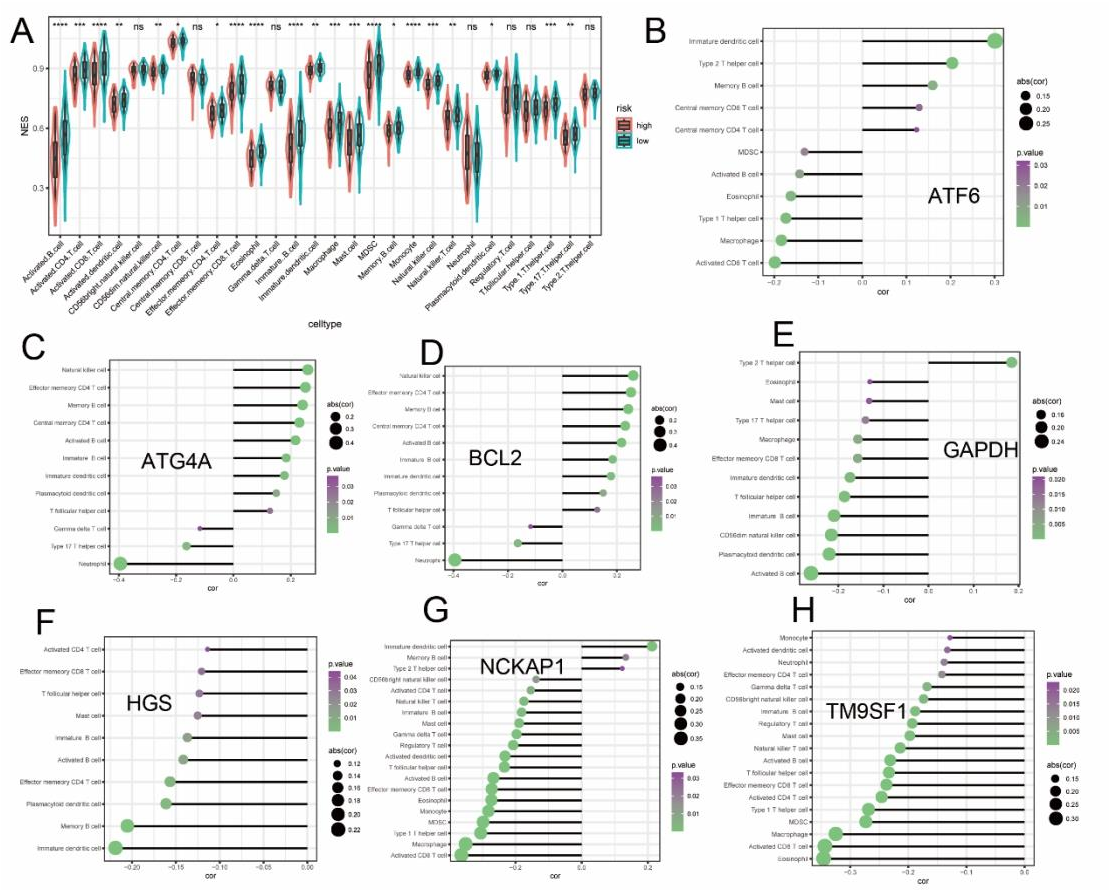

Figure11: Based on the relationship between 7 autophagy gene models and immune cells. (A): Analysis of the difference between the high and low risk groups in 28 immune cells, calculate the p value with Wilcoxon test and add it as an asterisk at the top of the picture.

(B-H): Correlation between autophagy gene and immune cells. Spearman method was used to calculate the correlation between 7 autophagy genes and immune cells, and the immune cells with $p < 0.05$ were selected.

Preprints (www.preprints.org) | NOT PEER-REVIEWED | Posted: 21 August 2020 doi:10.20944/preprints202008.0476.v1

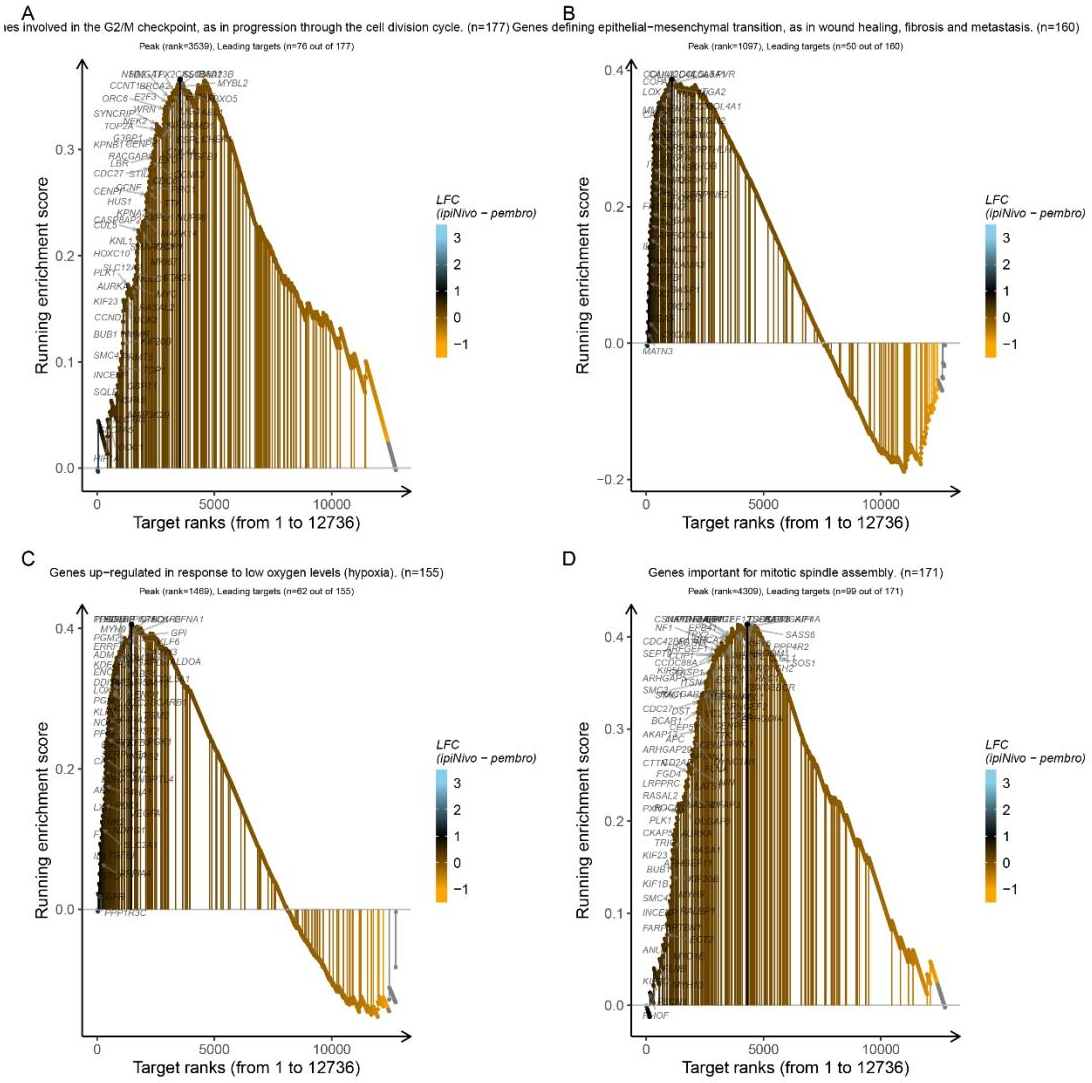

Figure12: GSEA analysis for high and low risk groups. (A): Mainly enriched in the G2/M checkpoint, as in progression through the cell division cycle. The genes marked in black are the dominant genes. (B): Mainly enriched in the Genes defining epithelial-mesenchymal transition, as in wound healing, fibrosis and metastasis. The genes marked in black are the dominant genes. (C): Mainly enriched in the Genes up-regulated in response to low oxygen levels (hypoxia). The genes marked in black are the dominant genes.(D): Mainly enriched in the Genes important for mitotic spindle assembly. The genes marked in black are the dominant genes.